



1 The suspended small-particles layer in the suboxic Black Sea: a proxy 2 for delineating the effective N₂-yielding section

3 Rafael Rasse¹, Hervé Claustre¹, and Antoine Poteau¹

4 ¹Sorbonne Université and CNRS, Laboratoire d'Océanographie de Villefranche (LOV) UMR7093, Institut de la Mer de
5 Villefranche (IMEV), 06230, Villefranche-sur-Mer, France.

6

7 Correspondence to: rafael.rasse@obs-vlfr.fr; rjrasse@gmail.com

8 **Abstract.** Upper suboxic water masses confine a majority of the microbial communities that can produce up to 90% of oceanic
9 N₂. This effective N₂-yielding section encloses a suspended small-particle layer, inferred from particle backscattering (b_{pp})
10 measurements. It is thus hypothesized that this layer (hereafter, the b_{pp} -layer) is linked to N₂-yielding microbial communities
11 such as anammox and denitrifying bacteria — a hypothesis yet to be evaluated. Here, data collected by three BGC-Argo floats
12 deployed in the Black Sea are used to investigate the origin of this b_{pp} -layer. To this end, we evaluate how key drivers of
13 anammox-denitrifying bacteria dynamics impact on the vertical distribution of b_{pp} and the thickness of the b_{pp} -layer. In
14 conjunction with published data on N₂ excess, our results suggest that the b_{pp} -layer is at least partially composed of anammox-
15 denitrifying bacteria for three main reasons: (1) strong correlations are recorded between b_{pp} and nitrate; (2) the top location
16 of the b_{pp} -layer is driven by the ventilation of oxygen-rich subsurface waters, while its thickness is modulated by the amount
17 of nitrate available to produce N₂; (3) the maxima of both b_{pp} and N₂ excess coincide at the same isopycnals where denitrifying-
18 anammox bacteria coexist. We thus advance that b_{pp} and O₂ can be exploited as a combined proxy to delineate the N₂-yielding
19 section of the Black Sea. This proxy can potentially contribute to refining delineation of the effective N₂-yielding section of
20 oxygen-deficient zones via data from the growing BGC-Argo float network.

21 1 Introduction

22 Suboxic water masses (O₂ ≤ 5 μM) host denitrifying and anammox bacteria that produce between 20-40% of oceanic N₂,
23 respectively via heterotrophic denitrification and anaerobic oxidation of ammonium (Gruber and Sarmiento, 1997; Ward
24 2013). The upper suboxic water masses of oceanic oxygen-deficient zones (ODZs) make up the most effective N₂-producing
25 section because this is where the bacteria that condition the process mainly develop (Ward et al., 2009; Dalsgaard et al.,
26 2012). For example, in such water masses in the open eastern tropical north Pacific, denitrifying and anammox bacteria can
27 generate up to 90% of the N₂ lost in the ODZ core (Babin et al., 2014). It is thus important to unravel the biogeochemical
28 parameters that trigger the accumulation of such bacteria in upper suboxic ODZs. This information is crucial for understanding
29 and quantifying how bacterial biomass and related N₂ loss can respond to the ongoing expansion of ODZs (Keeling and Garcia,
30 2002; Stramma et al., 2008; Helm et al., 2011; Schmidtko et al., 2017). Ultimately, greater accuracy in this domain can
31 contribute to improving mechanistic predictions on how such expansion affects the oceans' role in driving the Earth's climate
32 by sequestering atmospheric carbon dioxide (e.g. Oschlies et al., 2018).

33 In suboxic water masses, the biogeochemical factors that can affect the abundance of denitrifying and anammox bacteria are
34 the levels of O₂, organic matter (OM), nitrate (NO₃⁻), ammonium (NH₄⁺), and hydrogen sulfide (H₂S) (Murray et al., 1995;
35 Ward et al., 2008; Dalsgaard et al., 2014; Bristow et al., 2016). Therefore, to elucidate what triggers the confinement of such



36 bacteria, we need to investigate how the above biogeochemical factors drive their vertical distribution, with high temporal and
37 vertical resolution. To this end, we should develop multidisciplinary approaches that allow us to permanently monitor the full
38 range of biogeochemical variables of interest in suboxic ODZs.

39 Optical proxies of tiny particles can be applied as an alternative approach to assess the vertical distribution of N₂-yielding
40 microbial communities in upper suboxic ODZs (Naqvi et al., 1993). For instance, anammox and denitrifying bacteria are found
41 as free-living bacteria (0.2-2 μm), and can be associated with small-suspended (> 2-30 μm), and large-sinking (> 30 μm)
42 particles (Fuchsman et al., 2012a, 2017; Ganesh et al., 2014, 2015). Therefore, particle backscattering (*b_{bp}*), a proxy for
43 particles in the ~ 0.2-20 μm size range (Stramski et al., 1999, 2004; Organelli et al., 2018), can serve to detect the presence of
44 these free-living bacteria and those associated with small-suspended particles.

45 Time series of *b_{bp}* acquired by biogeochemical Argo (BGC-Argo) floats highlight the presence of a permanent layer of
46 suspended small particles in upper suboxic ODZs (*b_{bp}-layer*) (Whitmire et al., 2009; Wojtasiewicz et al., 2018). It has been
47 hypothesized that this *b_{bp}-layer* is linked to N₂-yielding microbial communities such as denitrifying and anammox bacteria.
48 However, this hypothesis has not yet been clearly demonstrated. To address this, the first step is to evaluate: (1) potential
49 correlations between the biogeochemical factors that control the presence of the *b_{bp}-layer* and denitrifying-anammox bacteria
50 (O₂, NO₃⁻, OM, H₂S, Murray et al., 1995; Ward et al., 2008; Dalsgaard et al., 2014; Bristow et al., 2016), and (2) the possible
51 relationship between the *b_{bp}-layer* and N₂ produced by microbial communities.

52 This first step is thus essential for identifying the origin of the *b_{bp}-layer* and, ultimately, determining if BGC-Argo observations
53 of *b_{bp}* can be implemented to delineate the suboxic zone where such bacteria are confined. The Black Sea appears as a suitable
54 area for probing into the origin of the *b_{bp}-layer* in suboxic waters in this way. It is indeed a semi-enclosed suboxic-anoxic basin
55 where N₂ production and related denitrifying and anammox bacteria are mainly confined within a well-defined suboxic zone
56 (Kuypers et al., 2003; Konovalov et al., 2005; Kirkpatrick et al., 2012). In addition, a permanent *b_{bp}-layer* is a typical
57 characteristic of this region (Stanev et al., 2017, 2018).

58 The goal of our study is therefore to investigate the origin of the *b_{bp}-layer* in the suboxic waters of the Black Sea using data
59 collected by BGC-Argo floats. More specifically, we aim to evaluate, within the suboxic zone, how: (1) two of the main factors
60 (O₂ and NO₃⁻) that drive the dynamics of denitrifying and anammox bacteria, impact on the location and thickness of the *b_{bp}-*
61 *layer*, (2) NO₃⁻ controls the vertical distribution of *b_{bp}* within this layer, (3) temperature drives the formation of the *b_{bp}-layer*
62 and consumption rates of NO₃⁻, and (4) particle content inferred from *b_{bp}* and N₂ produced by microbial communities are at
63 least qualitatively correlated. Ultimately, our findings allow us to infer that *b_{bp}* can potentially be used to detect the presence
64 of the microbial communities that drive N₂ production in the upper suboxic waters masses – including denitrifying-anammox
65 bacteria.

66 2 Methods

67 2.1 Bio-optical and physicochemical data measured by BGC-Argo floats

68 We used data collected by three BGC-Argo floats that profiled at a temporal resolution of 5-10 days in the first 1000 m depth
69 of the Black Sea from December 2013 to July 2019 (Figure 1). These floats — allocated the World Meteorological
70 Organization (WMO) numbers 6900807, 6901866, and 7900591 — collected 239, 301, and 518 vertical profiles, respectively.
71 BGC-Argo float 6901866 was equipped with four sensors: (1) a SBE-41 CP conductivity-T-depth sensor (Sea-Bird Scientific),
72 (2) an Aanderaa 4330 optode (serial number:1411), (3) a WETLabs ECO Triplet Puck, and (4) a Satlantic Submersible



73 Ultraviolet Nitrate Analyzer (SUNA). These sensors measured upward profiles of: (1) temperature (T), conductivity, and
74 depth, (2) dissolved oxygen (O_2), (3) chlorophyll fluorescence, total optical backscattering (particles + pure seawater) at 700
75 nm and fluorescence by Colored Dissolved Organic Matter, and (4) nitrate (NO_3^-) and bisulfide (HS^-). Floats 6900807 and
76 7900591 were equipped with only the first three sensors.

77 Raw data of fluorescence and total backscattering were converted into Chlorophyll concentration (*chl*) and particle
78 backscattering (b_{bp}) following standard protocols (Schmechtig et al., 2014, 2015). Spike signals in vertical profiles of *chl* and
79 b_{bp} and due to particle aggregates were removed by using a median filter with a window size of three data points (Briggs et al.,
80 2011). NO_3^- , HS^- and O_2 data were processed following BGC-Argo protocols (Johnson et al., 2018; Thierry et al., 2018).
81 Sampling regions covered by the three floats encompassed most of the Black Sea area (Figure 1, and Appendix A). However,
82 we only used data collected during periods without a clear injection of small particles derived from the productive layer and
83 Bosphorus plume (e.g. advection of water masses, Stanev et al., 2017). This restriction allowed us to focus on the *in-situ* 1D
84 processes driving local formation of the b_{bp} -layer, with minimal interference from any possible external sources of small
85 particles.

86 We only describe the time series of data collected by float 6901866 because this was the only float carrying a NO_3^-/HS^- sensor.
87 Data acquired by floats 6900807 and 7900591 are described in Appendix A, and nevertheless used as complementary data to
88 those of float 6901866 to corroborate: (1) qualitative correlations between O_2 levels and the location of the b_{bp} -layer, and (2)
89 consistency in the location of the b_{bp} maximum within the b_{bp} -layer.

90 2.2 Defining the suboxic zone, mixed layer depth, and productive layer

91 We used O_2 and NO_3^- to respectively define the top and bottom isopycnals of the suboxic zone where denitrifying and anammox
92 bacteria are expected to be found. To set the top isopycnal, we applied an O_2 threshold of $\sim 3 \mu M$ because denitrifying and
93 anammox bacteria seem to tolerate O_2 concentrations beneath this threshold (Jensen et al., 2008; Babbín et al., 2014). The
94 bottom isopycnal was defined as the deepest isopycnal at which NO_3^- was detected by the SUNA sensor ($0.23 \pm 0.32 \mu M$).
95 NO_3^- was used to set this isopycnal because heterotrophic denitrification and subsequent reactions cannot occur without NO_3^-
96 (Lam et al., 2009; Bristow et al., 2017). HS^- was not used to delimit the bottom of this zone because the maximum concentration
97 of H_2S that denitrifying and anammox bacteria tolerate is not well established (Murray et al., 1995; Kirkpatrick et al., 2012;
98 see also section 3.1).

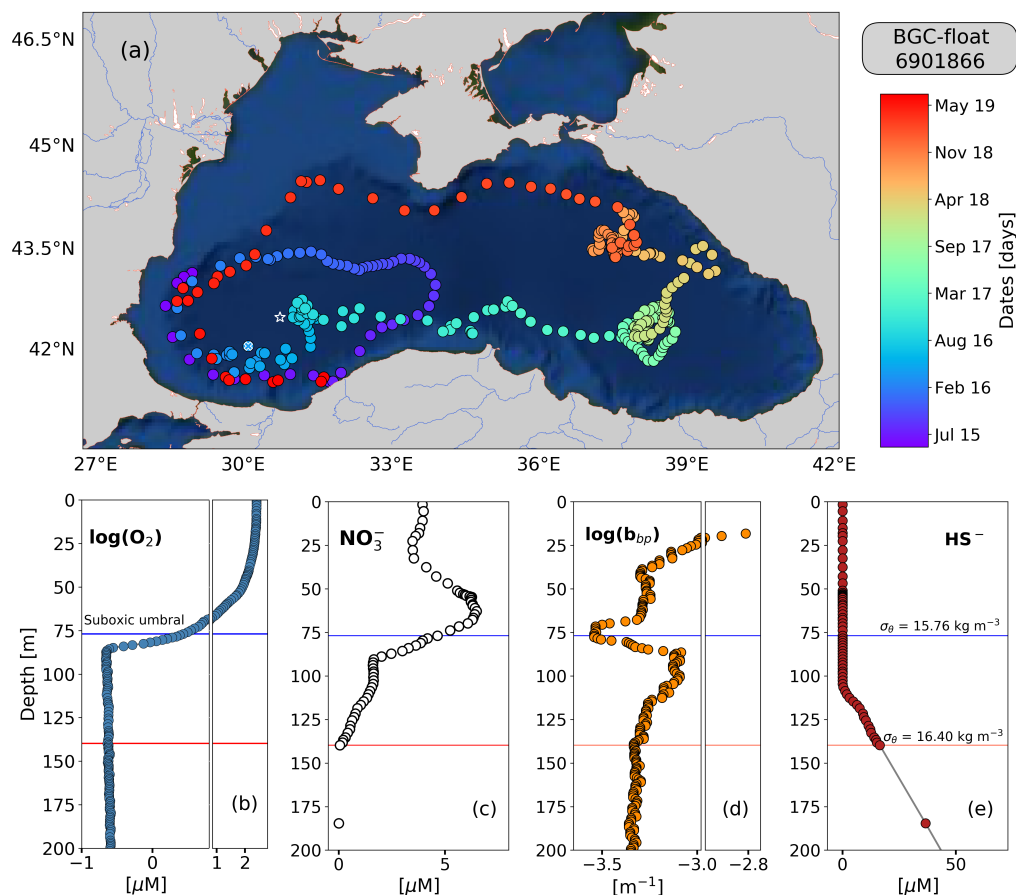
99 Mixed layer depth (MLD) was computed as the depth at which density differed from 0.03 kg m^{-3} with respect to the density
100 recorded at 1m depth (de Boyer Montégut et al., 2004). We used *chl* to define the productive layer where living phytoplankton
101 were present and producing particulate organic carbon. The base of this layer was set as the depth at which *chl* decreased
102 below 0.25 mg m^{-3} . This depth was used only as a reference to highlight the periods when surface-derived small particles were
103 clearly injected into the suboxic zone.

104 2.3 Complementary cruise data on N_2 excess and NO_3^-

105 Published data on $N_2:Ar$ ratios and NO_3^- collected at the southwest of the Black Sea in March 2005 (Fuchsman et al., 2008,
106 2019) were exploited to complement discussion of our results. N_2 produced by anaerobic microbial communities (N_2 excess,
107 μM) was estimated from $N_2:Ar$ ratios and argon concentrations at atmospheric saturation (Hamme and Emerson, 2004). N_2
108 excess data were used to: (1) describe the suboxic zone where N_2 is expected to be predominantly produced, and (2) highlight



109 qualitative correlations between N_2 excess, the location of the b_{bp} -layer, and vertical distribution of small particles within the
 110 b_{bp} -layer.



111
 112 **Figure 1:** (a) Sampling locations of float 6901866 between May 2015 and July 2019. Colored circles indicate the date
 113 (color bar) for a given profile. The white star in (a) marks the sampling site of the cruise (March 2005). The white x in
 114 (a) highlights the float location on 6th April 2016. Float profiles of (b) $\log(O_2)$, (c) NO_3^- , (d) $\log(b_{bp})$, and (e) HS^- collected
 115 on 24th November 2018.

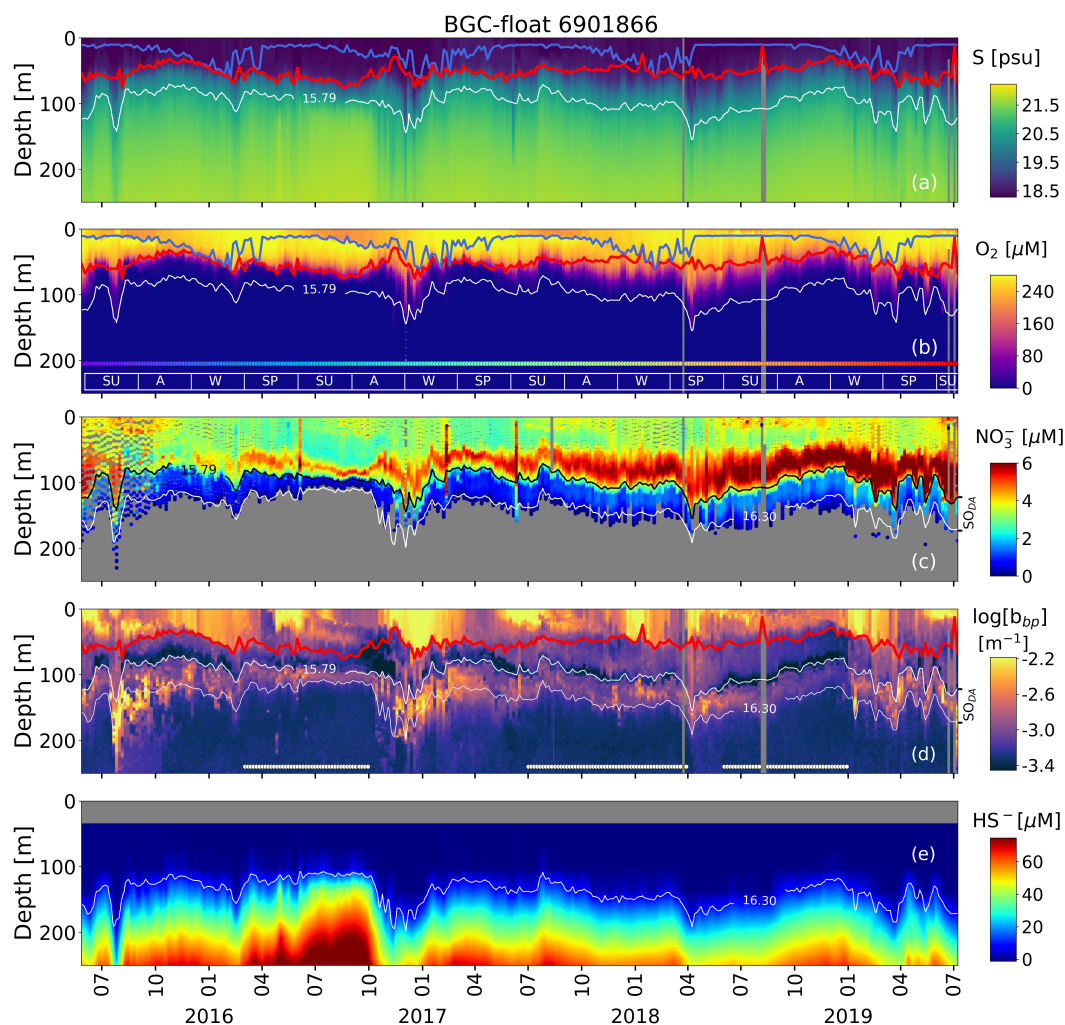
116 3 Results and discussion

117 3.1 Description of the suboxic zone

118 The top and bottom of the suboxic zone are located around the isopycnals (mean \pm standard deviation) $15.79 \pm 0.23 \text{ kg m}^{-3}$
 119 and $16.30 \pm 0.09 \text{ kg m}^{-3}$, respectively. The two isopycnals therefore delimit the suboxic zone where denitrifying and anammox
 120 bacteria are expected to be found (zone hereafter called $SO_{D,A}$, Figure 2). The top location and thickness of the $SO_{D,A}$ show
 121 large spatial-temporal variability, ranging between 80–180 m and 30–80 m, respectively (Figure 2). The bottom of the $SO_{D,A}$ is
 122 slightly sulfidic ($HS^- = 11.4 \pm 3.53 \text{ } \mu\text{M}$, $n = 86$) and deeper than suggested (e.g. $\sigma_\theta = 16.20 \text{ kg m}^{-3}$, and $H_2S \leq 10 \text{ nM}$, Murray



123 et al., 1995). However, our results coincide with the slightly sulfidic conditions of the deepest isopycnal at which anammox
 124 bacteria can be still recorded ($\sigma_\theta = 16.30 \text{ kg m}^{-3}$, and $\text{H}_2\text{S} \geq 10 \text{ }\mu\text{M}$, Kirkpatrick et al., 2012).



125
 126 **Figure 2:** Time series of: (a) Salinity (S), (b) O_2 , (c) NO_3^- , (d) $\log(b_{bp})$, and (e) HS^- . The blue lines in (a) and (b) indicate
 127 the mixed layer depth. The red lines in (a), (b) and (d) show the base of the productive region. The isopycnals 15.79 kg m^{-3} and 16.30 kg m^{-3} describe the top and bottom of the suboxic zone (SO_{D-A}), respectively. SU, A, W, and SP stand for
 128 summer, autumn, winter, and spring, respectively. The colored horizontal line in (b) indicates the sampling site for a
 129 given date (Figure 1). The horizontal white lines in (d) are the profiles used to: (1) delimit the SO_{D-A} , and (2) compute
 130 correlations between b_{bp} , NO_3^- , and T within the SO_{D-A} .
 131

132 3.2 NO_3^- and O_2 as key drivers of the thickness and location of the suspended small-particle layer

133 The permanent b_{bp} -layer is always confined within the two isopycnals that delimit the SO_{D-A} (Figure 2). It follows that the
 134 thickness and top location of this layer demonstrate the same spatial and temporal variability as the one described for the SO_D .



135 σ_{θ} (Figure 2 and Appendix A). This correlation indicates that variations in the thickness and top location of the b_{bp} -layer are
136 partially driven, respectively, by: (1) the amount of NO_3^- available to produce N_2 inside the $SO_{D,A}$, and (2) downward ventilation
137 of oxygen-rich subsurface waters (Figure 2 and Appendix A).

138 NO_3^- and O_2 are two of the key factors that modulate the presence of denitrifying and anammox bacteria (Ulloa et al., 2012;
139 Bristow et al., 2017). Therefore, the results described above highlight that at least a fraction of the b_{bp} -layer should be due to
140 these bacteria. This notion is supported by three main observations. Firstly, the top location of the b_{bp} -layer is driven by the
141 intrusion of subsurface water masses ($S \leq 20.36 \pm 0.18$ psu) with O_2 concentrations above the levels tolerated by denitrifying
142 and anammox bacteria ($\text{O}_2 \geq 3 \mu\text{M}$, Jensen et al., 2008; Babbin et al., 2014; Figure 2). As a result, in regions where O_2 is
143 ventilated to deeper water masses, the top location of the b_{bp} -layer is also deeper. The contrary is observed when O_2 ventilation
144 is shallower (Figure 2 and Appendix A). Secondly, denitrifying and anammox bacteria reside between the isopycnals 15.60-
145 16.30 kg m^{-3} (Fuchsman et al., 2012a; Kirkpatrick et al., 2012), while the b_{bp} -layer is formed between isopycnals ~15.79-16.30
146 kg m^{-3} . We can thus infer coexistence of such bacteria between the coincident isopycnals where the b_{bp} -layer is generated.
147 Thirdly, NO_3^- declines from around isopycnal 15.79 kg m^{-3} to the isopycnal 16.30 kg m^{-3} due to the expected N_2 production
148 (Figures 2-3, and Kirkpatrick et al., 2012).

149 Overall, the qualitative evidence presented above points out that denitrifying and anammox bacteria are likely to represent at
150 least a fraction of the b_{bp} -layer. However, it is also known that these bacteria produce N_2 coupled with sulfur-oxidizing bacteria,
151 and generate inorganic particles as intermediaries (e.g. MnOx , Johnson, 2006; Canfield et al., 2010; Fuchsman et al., 2012b;
152 Callbeck et al., 2018; Stanev et al., 2018). Ultimately, both bacteria communities and inorganic particles appear to contribute
153 to the formation of the b_{bp} -layer. This observation leads us to argue, in the next section, that the b_{bp} -layer is partially composed
154 of N_2 -yielding microbial communities such as *anammox* and *denitrifying* bacteria.

155 3.3 Role of the removal rate of NO_3^- and of temperature in the vertical distribution of small particles

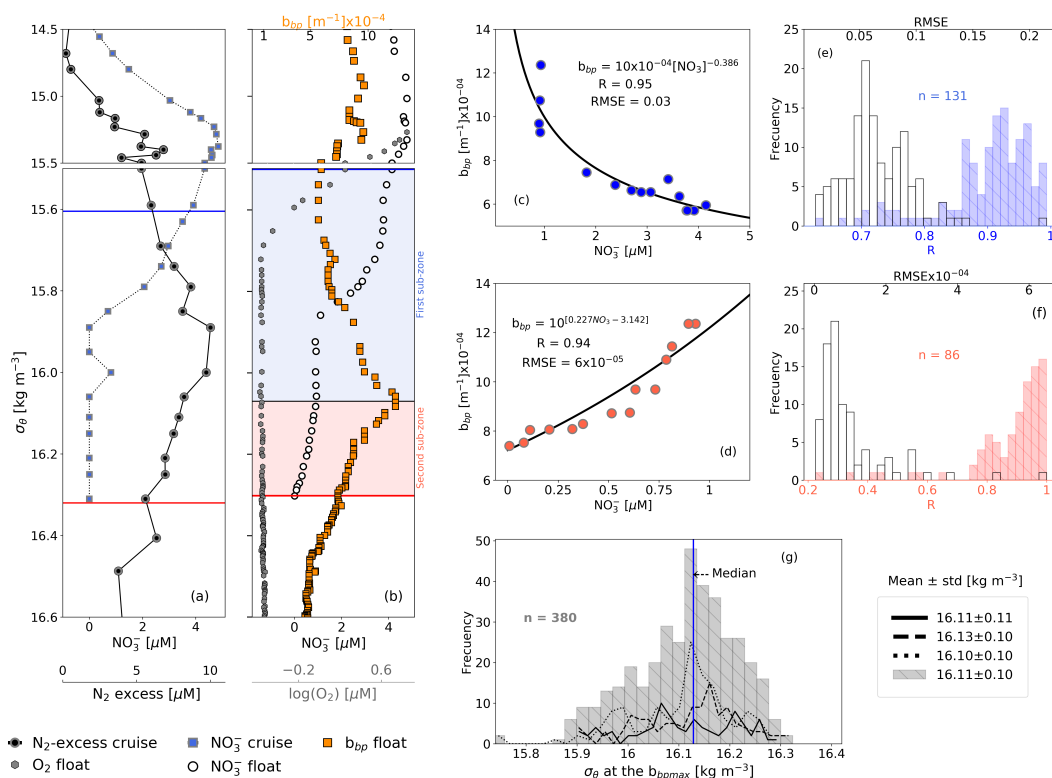
156 We propose that the removal rate of NO_3^- is a key driver of the vertical distribution of small particles and N_2 excess within the
157 $SO_{D,A}$. This is because the vertical profiles of small particles and of N_2 excess are qualitatively similar, and both profiles are
158 clearly related to the rate at which NO_3^- is removed from the $SO_{D,A}$ (Figures 3-4). For instance, maxima of N_2 excess and b_{bp}
159 coincide around the isopycnal $16.11 \pm 0.11 \text{ kg m}^{-3}$ (Figure 3, Konovalov et al., 2005; Fuchsman et al., 2008, 2019). At this
160 isopycnal, the mean concentration of NO_3^- is $1.19 \pm 0.53 \mu\text{M}$. We thus propose that this NO_3^- threshold value splits the $SO_{D,A}$
161 in two sub-zones with distinctive biogeochemical conditions. Ultimately, these two different sets of conditions drive the rates
162 at which NO_3^- and small particles are removed and formed within the $SO_{D,A}$, respectively (Figure 3, and explanation below).

163 The first sub-zone is thus located between the top of the $SO_{D,A}$ ($\sigma_{\theta} = 15.79 \text{ kg m}^{-3}$) and around the isopycnal 16.11 kg m^{-3} .
164 Here, removal rates of NO_3^- ($-0.16 \pm 0.10 \mu\text{M m}^{-1}$, Figure 4) are likely to be boosted by: (1) high content of organic matter
165 (dissolved organic carbon = $122 \pm 9 \mu\text{M}$, Margolin et al., 2016) and NO_3^- ($\geq 1.19 \pm 0.53 \mu\text{M}$), and (2) O_2 levels staying between
166 a range that maintain the yielding of N_2 ($0.24 \pm 0.04 \mu\text{M} \geq \text{O}_2 \leq 2.8 \pm 0.14 \mu\text{M}$, $n = 100$, the means of the minima and maxima
167 of O_2 , respectively, in the first sub-zone). Consequently, the formation of small particles (and related N_2 excess) increases from
168 the top of the $SO_{D,A}$ to around the isopycnal 16.11 kg m^{-3} (Figure 3). This hypothesis is in part confirmed by significant and
169 negative power-law correlations between the suspended small-particle content and NO_3^- in this sub-zone (Figure 3).

170 The second sub-zone is located between isopycnal 16.11 kg m^{-3} and the bottom of the $SO_{D,A}$ ($\sigma_{\theta} = 16.30 \text{ kg m}^{-3}$, Figure 3).
171 Here, NO_3^- is low ($\leq 1.19 \pm 0.53 \mu\text{M}$) and O_2 is relatively constant ($0.23 \pm 0.02 \mu\text{M}$, $n = 2284$, mean of O_2 calculated in the
172 second sub-zone for all profiles). These constant levels of O_2 roughly correspond to those at which anammox and heterotrophic



173 denitrification are inhibited by $\sim 50\%$ ($0.21 \mu\text{M}$, and $0.81 \mu\text{M}$, respectively, Dalsgaard et al., 2014). As a result, this sub-zone
 174 exhibits a decline in removal rates of NO_3^- ($-0.04 \pm 0.01 \mu\text{M m}^{-1}$, Figure 4) along with inhibited formation of small particles.
 175 Ultimately, both the content of small particles and related N_2 excess decrease from around isopycnal 16.11 kg m^{-3} to the bottom
 176 of the SO_{D-A} (Figure 3). These results are in agreement with significant and positive exponential correlations computed between
 177 the small-particle content inferred from b_{bp} and NO_3^- within this sub-zone (Figure 3).



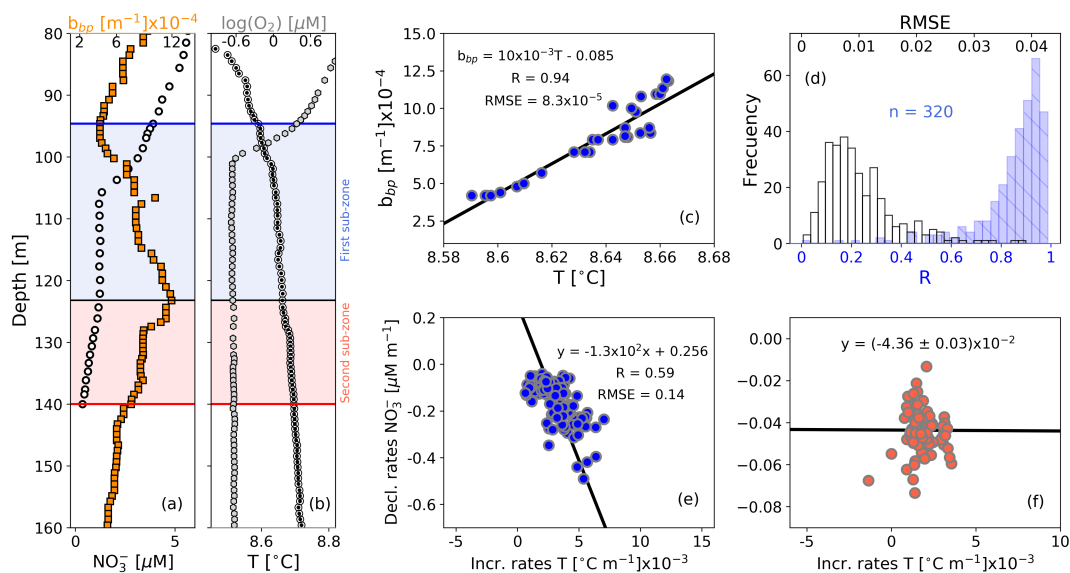
178

179 **Figure 3:** (a) Cruise profiles of NO_3^- , and N_2 excess, collected in March 2005 (Fuchsman et al., 2019). (b) Float profiles
 180 of NO_3^- , b_{bp} , and $\log(\text{O}_2)$ measured on 6th April 2016. Profiles in (a) and (b) were conducted at the northwest of the basin
 181 (see Figure 1). The top and bottom of the SO_{D-A} are described in (a) and (b) as horizontal blue and red lines, respectively.
 182 The b_{bp} maximum is the horizontal black line in (b). The first and second sub-zone of the SO_{D-A} are respectively
 183 highlighted in (b) as blue and red squares. NO_3^- vs b_{bp} in (c) the first, and (d) the second sub-zone, of the float profile in
 184 (b). The number of data points visualized in (c) is lower than in (b) for the first sub-zone because b_{bp} and NO_3^- are not
 185 always recorded at the same depths. (e) Frequency distributions of correlation coefficients (R, blue bars), and root
 186 mean square errors (RMSE, white bars) for NO_3^- vs b_{bp} in the first sub-zone. (f) Same as (e) but for the second sub-zone.
 187 (g) Frequency distributions of the isopycnals at which b_{bp} maxima are found within the SO_{D-A} . Dotted, dashed, and solid
 188 black lines in (g) are data collected by floats 7900591, 6901866, and 6900807, respectively. Gray bars include all data.

189 Strong-positive linear correlations are also recorded between b_{bp} and T in the first sub-zone of the SO_{D-A} (Figure 4). This is
 190 likely to indicate that the formation of small particles is sensitive to very tiny increments in T ($0.003 \pm 0.001 \text{ }^\circ\text{C m}^{-1}$, $n = 133$).
 191 We thus infer a tendency for the decline rates of NO_3^- and related production of N_2 to increase with T. This hypothesis is at
 192 least partially supported by the significant correlation between NO_3^- decline rates and T increase rates in this sub-zone (Figure



193 4). Within the second sub-zone, T continues increasing while b_{bp} decreases, likely due to inhibition of the formation of small
 194 particles for the reasons described above (Figure 4). These observations suggest that the production of small particles is likely
 195 to have first- and second-order covariations, with NO_3^- and T, respectively — a likelihood backed up by a lack of correlation
 196 between NO_3^- decline rates and T increase rates in this sub-zone (Figure 4). However, we admittedly cannot discount the
 197 possibility that the decline in b_{bp} may also be due to the dissolution of MnOx just beneath the isopycnal 16.11 kg m^{-3} (e.g.
 198 Kononov et al., 2003, 2005, 2006).



199
 200 **Figure 4:** Float profiles of (a) NO_3^- and b_{bp} , and (b) T and $\log(\text{O}_2)$ collected on 10th September 2017. Horizontal blue
 201 and red lines in (a) and (b) are the top and bottom of the SO_{D-A} . The b_{bp} maximum is indicated in (a) and (b) as horizontal
 202 black lines. The first and second sub-zones of the SO_{D-A} are respectively highlighted in (a) and (b) as blue and red
 203 squares. (c) b_{bp} vs T for the first sub-zone of the profile in (b). (d) Frequency distributions of correlation coefficients (R,
 204 blue bars), and root mean square errors (RMSE, white bars), for b_{bp} vs T in the first sub-zone, including data collected
 205 by the three floats. Decrease rates of NO_3^- vs increase rates of T in (e) the first and (f) the second sub-zone.

206 To summarize, BGC-Argo float data combined with a proxy of N_2 production suggest that the b_{bp} -layer is at least partially
 207 composed of anaerobic microbial communities involved in the production of N_2 . It is thus inferred that this b_{bp} -layer includes
 208 *anammox* and *denitrifying* bacteria. These results also suggest that N_2 production rates can be highly variable in the Black Sea
 209 because the characteristics of the b_{bp} -layer show large spatial-temporal variations driven by changes in NO_3^- and O_2 (Figures 2
 210 and 4). Finally, we propose that b_{bp} and O_2 can be exploited as a combined proxy for defining the N_2 -producing section of the
 211 suboxic Black Sea. We consider that this combined proxy can delineate the top and base of this section, by applying an O_2
 212 threshold of 3.0 μM , and the bottom isopycnal of the b_{bp} -layer, respectively. This section should thus be linked to free-living
 213 bacteria (0.2-2 μm), and those associated with small-suspended particles (> 2-20 μm).



214 **3.4 New perspectives for studying N₂ losses in suboxic ODZs**

215 The conclusions and inferences of this study, especially those related to the origin and drivers of the *b_{bp}*-layer, primarily apply
216 to the Black Sea. However, these findings may also have a wider application. In particular, suboxic ODZs are similarly
217 characterized by the formation of a layer of suspended small particles that can be optically detected by *b_{bp}* and the attenuation
218 coefficients of particles (Spinrad et al., 1989; Naqvi et al., 1993; Whitmire et al., 2009). This layer is linked to N₂-yielding
219 microbial communities because its location coincides with the maxima of N₂ excess, microbial metabolic activity, and nitrite
220 (NO₂⁻, the intermediate product of denitrification-anammox that is mainly accumulated in the N₂-yielding section, Spinrad
221 et al., 1989; Naqvi et al., 1991, 1993; Devon et al., 2006; Chang et al., 2010, 2012; Ulloa et al., 2012; Wojtasiewicz et al., 2018).
222 Therefore, our findings suggest that highly resolved vertical profiles of *b_{bp}* and O₂ can potentially be used as a combined proxy
223 to define the *effective* N₂-production section of suboxic ODZs. Such definition can be key to better-constrained global estimates
224 of N₂ loss rates because it can allow us to: (1) accurately predict the suboxic water volume where around 90% of N₂ is produced
225 in the ODZ core (Babin et al., 2014), and (2) evaluate how the location and thickness of the N₂-yielding section vary due to
226 changes in the biogeochemical factors that modulate anammox and heterotrophy denitrification.

227 Global estimates of N₂ losses differ by 2-3 fold between studies (e.g. 50-150 Tg N yr⁻¹, Codispoti et al., 2001; Bianchi et al.,
228 2012, 2018; DeVries et al., 2012; Wang et al., 2019). These discrepancies are caused in part by inaccurate estimations of the
229 suboxic volume of the N₂-production section. Other sources of uncertainties arise from the methods applied to estimate the
230 amount of POC that fuels N₂ production. For instance, POC fluxes and their subsequent attenuation rates are not well resolved
231 because they are computed respectively from satellite-based primary-production algorithms and generic power-law functions
232 (Bianchi et al., 2012, 2018; DeVries et al., 2012). POC-flux estimates based on these algorithms visibly exclude: (1) POC
233 supplied by zooplankton migration (Kiko et al., 2017; Tutasi and Escribano, 2020), (2) substantial events of POC export
234 decoupled from primary production (Karl et al., 2012), and (3) the role of small particles derived from the physical and
235 biological fragmentation of larger ones (Karl et al., 1988; Briggs et al., 2020). In addition, these estimates do not take into
236 consideration the inhibition effect that O₂ intrusions may have on N₂-yield rates (Whitmire et al., 2009; Ulloa et al., 2012;
237 Dalsgaard et al., 2014; Peters et al., 2016).

238 Overall, mechanistic predictions of N₂ losses misrepresent the strong dynamics of the biogeochemical and physical processes
239 that regulate them. Consequently, it is still debated whether the oceanic nitrogen cycle is in balance or not (Codispoti 2007;
240 Gruber and Galloway 2008; DeVries et al., 2012; Jayakumar et al., 2017; Bianchi et al., 2018; Wang et al., 2019). The subsiding
241 uncertainty points to a compelling need for alternative methods that allow accurate refinement of oceanic estimations of N₂
242 losses.

243 Our study supports the proposition that robotic observations of *b_{bp}* and O₂ can be used to better delineate the N₂-yielding section
244 at the appropriate spatial (e.g. vertical and regional) and temporal (e.g. event, seasonal, interannual) resolutions. In addition,
245 POC fluxes can be simultaneously quantified using the same float technology (BGC-Argo, Bishop et al., 2009; Dall'Olmo and
246 Mork 2014; Boyd et al., 2019; Estapa et al., 2019; Rasse and Dall'Olmo 2019). These robotic measurements can contribute to
247 refining global estimates of N₂ losses by better constraining both the suboxic zone where N₂ is produced, and POC fluxes that
248 fuel its loss. Ultimately, O₂ intrusions into the N₂-yielding section can potentially be quantified by BGC-Argo floats to assess
249 their regulatory effect on N₂ losses.



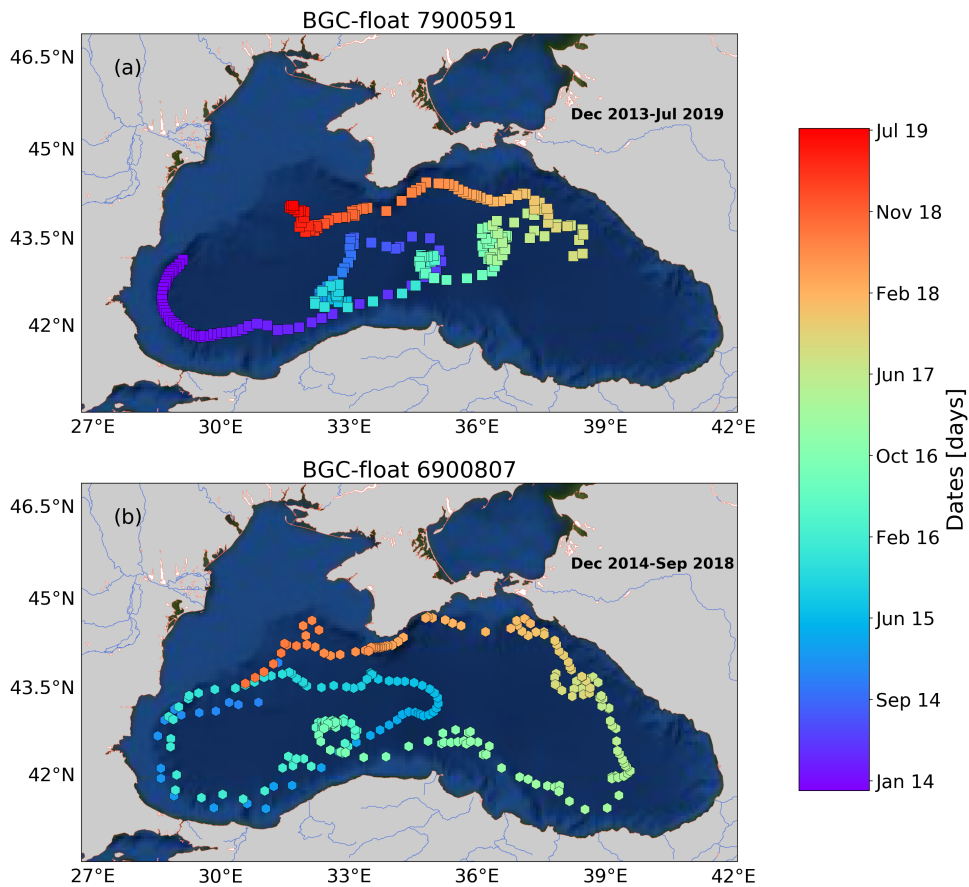
250 **Conclusions**

251 Our results suggest that the *b_{np}-layer* of the suboxic Black Sea is at least partially composed of anammox and denitrifying
252 bacteria. The location and thickness of this layer show strong spatial-temporal variability, mainly driven by the ventilation of
253 oxygen-rich subsurface waters, and nitrate available to generate N₂, respectively. Such variations in the characteristics of the
254 *b_{np}-layer* highlight that N₂-production rates can be highly variable in the Black Sea. We therefore propose that high resolution
255 measurements of O₂ and *b_{np}* can potentially be exploited as a combined proxy to delineate the *effective* N₂-yielding section of
256 ODZs. This proposition is in part supported by evidence that the *b_{np}-layer* and a majority of N₂-yielding microbial communities
257 are both confined in upper suboxic ODZs. We however recommend investigation into the key biogeochemical drivers of the
258 *b_{np}-layer* for each ODZ. This information will be critical for validating the applicability of the *b_{np}-layer* in assessing spatial-
259 temporal changes in N₂ production.

260 Finally, it is evident that BGC-Argo float observations can acquire essential proxies of N₂ production and associated drivers
261 at appropriate spatial and temporal resolutions. The development of observation-modeling synergies therefore holds the
262 potential to deliver an unprecedented view of N₂-loss drivers if robotic observations become an integrated part of model
263 validation. Ultimately, this approach could prove essential for reducing present uncertainties in the oceanic N₂ budget.



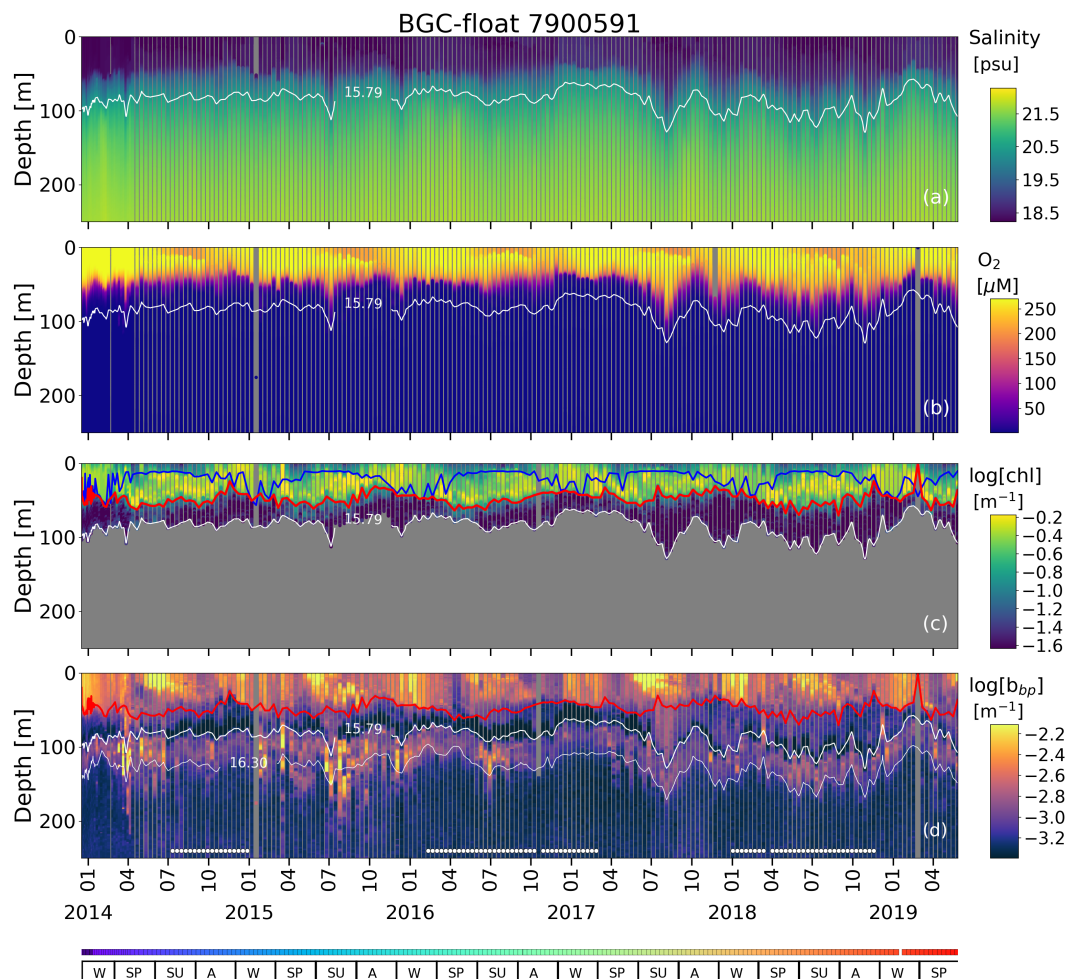
264 **Appendix A: Supplementary Figures**



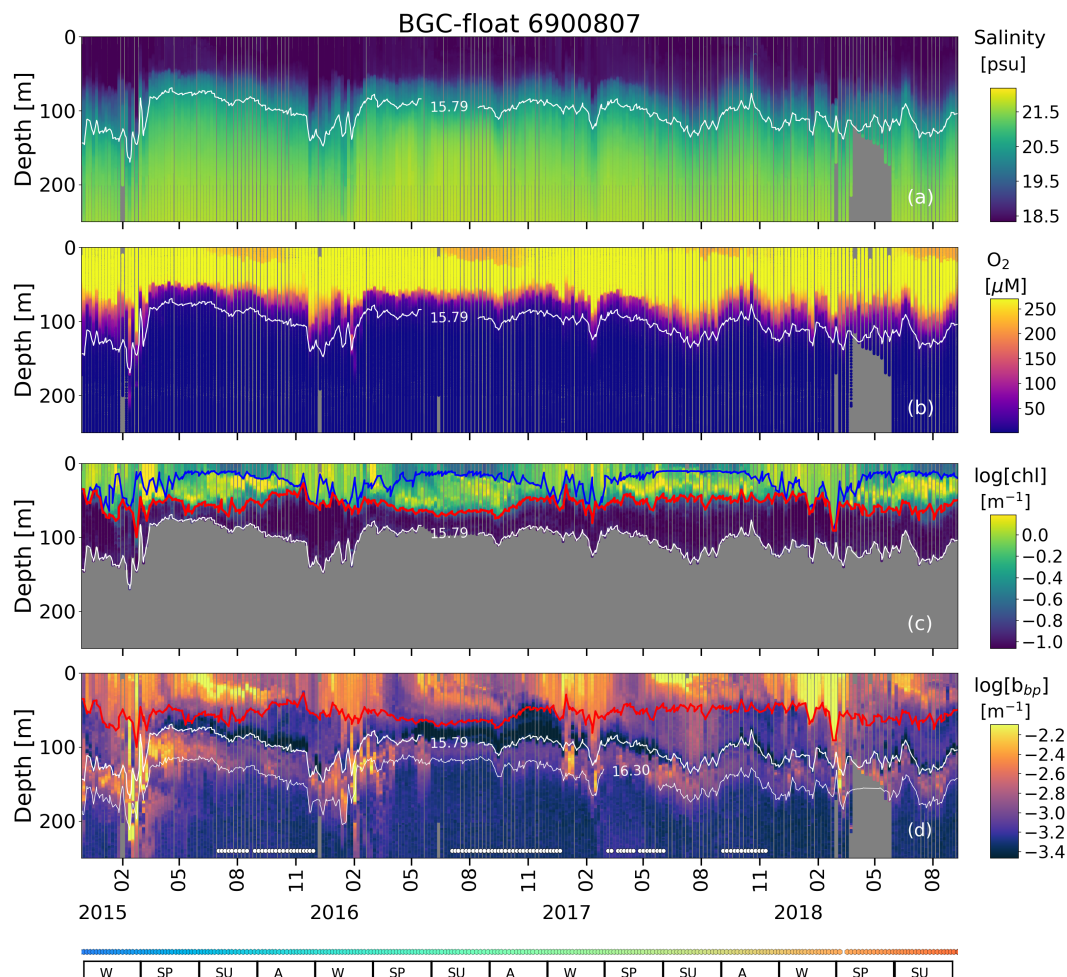
265

266 **Figure A1: Sampling locations of floats (a) 7900591 and (b) 6900807 between December 2013 and July 2019. Colored**

267 **squares and hexagons indicate the date (colorbar) for a given profile of floats 6900807 and 7900591, respectively.**



268
 269 **Figure A2:** Time series of (a) S, (b) O₂, (c) log(*chl*), and (d) log(*b_{bp}*) for float 7900591. The blue line in (c) indicates the
 270 mixed layer depth. The red lines in (c) and (d) show the base of the productive region. The isopycnals 15.79 kg m⁻³ and
 271 16.30 kg m⁻³ describe the top and bottom of the suboxic zone (*SO_{D-A}*), respectively. SU, A, W, and SP stand for summer,
 272 autumn, winter, and spring, respectively. The colored horizontal line at the bottom indicates the sampling site for a
 273 given date (Figure S1). The horizontal white lines in (d) are the profiles used to: (1) delimit the *SO_{D-A}*, and (2) find the
 274 isopycnals at which *b_{bp}* is maximum in the *SO_{D-A}*. *chl* is set to zero in the *SO_{D-A}* due to fluorescence contamination (Stanev
 275 et al., 2017).



276

277 **Figure A3: Same as Figure A2 but for float 6900807**

278 *Data availability.* Data from Biogeochemical-Argo floats used in this study are freely available at <ftp.ifremer.fr/ifremer/argo>.
 279 These data were collected and made freely available by the International Argo Program and the national programs that
 280 contribute to it (<http://www.argo.ucsd.edu>; the Argo Program is part of the Global Ocean Observing System). Data on $N_2:Ar$
 281 ratios are freely available at <https://agupubs.onlinelibrary.wiley.com/doi/abs/10.1029/2018GB006032>.

282 *Author contributions.* R.R. conceptualized the study, wrote the original draft, and generated all figures. H.C. contributed to
 283 tuning the study's conceptualization and figures design. A.P. processed all BGC-Argo float data. R.R. and H.C. reviewed and
 284 edited the final manuscript.

285 *Acknowledgments.* This study was conducted in the framework of the *Noceanic* project. This project is funded by the European
 286 Union's Horizon 2020 research and innovation program under the Marie Skłodowska-Curie Individual Fellowship awarded to
 287 Rafael Rasse (grant agreement 839062). This study is a contribution to the remOcean project (European Research Council,
 288 grant agreement 246777, Hervé Claustre).



- 289 *Competing interests.* The authors declare that they have no conflicts of interest.
- 290 **References**
- 291 Alldredge, A. L., and Cohen, Y.: Can microscale chemical patches persist in the sea? Microelectrode study of marine snow,
292 fecal pellets, *Science*, 235(4789), 689-691, DOI: 10.1126/science.235.4789.689, 1987
- 293 Altabet, M. A., Ryabenko, E., Stramma, L., Wallace, D. W., Frank, M., Grasse, P., and Lavik, G.: An eddy-stimulated hotspot
294 for fixed nitrogen-loss from the Peru oxygen minimum zone, *Biogeosciences*, 9, 4897-4908, [https://doi.org/10.5194/bg-9-](https://doi.org/10.5194/bg-9-4897-2012)
295 4897-2012, 2012
- 296 Babbín, A. R., Keil, R. G., Devol, A. H., and Ward, B. B.: Organic matter stoichiometry, flux, and oxygen control nitrogen
297 loss in the ocean, *Science*, 344(6182), 406-408, DOI: 10.1126/science.1248364, 2014.
- 298 Bianchi, D., Dunne, J. P., Sarmiento, J. L., and Galbraith, E. D.: Data-based estimates of suboxia, denitrification, and N₂O
299 production in the ocean and their sensitivities to dissolved O₂, *Global Biogeochem. Cy.*, 26(2), 2012.
- 300 Bianchi, D., Weber, T. S., Kiko, R., and Deutsch, C.: Global niche of marine anaerobic metabolisms expanded by particle
301 microenvironments, *Nat. Geosci.*, 11(4), 263-268, <https://doi.org/10.1038/s41561-018-0081-0>, 2018.
- 302 Bishop, J. K., and Wood, T. J.: Year-round observations of carbon biomass and flux variability in the Southern Ocean, *Global*
303 *Biogeochem. Cy.*, 23(2), <https://doi.org/10.1029/2008GB003206>, 2009.
- 304 Boyd, P. W., Claustre, H., Levy, M., Siegel, D. A., and Weber, T.: Multi-faceted particle pumps drive carbon sequestration in
305 the ocean, *Nature*, 568(7752), 327-335, <https://doi.org/10.1038/s41586-019-1098-2>, 2019.
- 306 Briggs, N., Perry, M. J., Cetinić, I., Lee, C., D'Asaro, E., Gray, A. M., and Rehm, E.: High-resolution observations of aggregate
307 flux during a sub-polar North Atlantic spring bloom, *Deep-Sea Res. Pt. I.*, 58(10), 1031–1039,
308 <https://doi.org/10.1016/j.dsr.2011.07.007>, 2011.
- 309 Briggs, N., Dall'Olmo, G., and Claustre, H.: Major role of particle fragmentation in regulating biological sequestration of CO₂
310 by the oceans, *Science*, 367(6479), 791-793, DOI: 10.1126/science.aay1790, 2020.
- 311 Bristow, L.A., Dalsgaard, T., Tiano, L., Mills, D.B., Bertagnolli, A.D., Wright, J.J., Hallam, S.J., Ulloa, O., Canfield, D.E.,
312 Revsbech, N.P. and Thamdrup, B.: Ammonium and nitrite oxidation at nanomolar oxygen concentrations in oxygen minimum
313 zone waters, *Proc. Natl. Acad. Sci. U. S. A.*, 113(38), 10601-10606, <https://doi.org/10.1073/pnas.1600359113>, 2016.
- 314 Bristow, L.A., Callbeck, C.M., Larsen, M., Altabet, M.A., Dekaezemacker, J., Forth, M., Gauns, M., Glud, R.N., Kuypers,
315 M.M., Lavik, G. and Milucka, J.: N₂ production rates limited by nitrite availability in the Bay of Bengal oxygen minimum
316 zone, *Nat. Geosci.*, 10(1), 24-29, <https://doi.org/10.1038/ngeo2847>, 2017.
- 317 Chang, B. X., Devol, A. H., and Emerson, S. R.: Denitrification and the nitrogen gas excess in the eastern tropical South
318 Pacific oxygen deficient zone, *Deep-Sea Res. Pt. I.*, 57(9), 1092-1101, <https://doi.org/10.1016/j.dsr.2010.05.009>, 2010.



- 319 Chang, B. X., Devol, A. H., and Emerson, S. R.: Fixed nitrogen loss from the eastern tropical North Pacific and Arabian Sea
320 oxygen deficient zones determined from measurements of $N_2:Ar$, *Global Biogeochem. Cy.*, 26(3),
321 <https://doi.org/10.1029/2011GB004207>, 2012.
- 322 Callbeck, C.M., Lavik, G., Ferdelman, T.G., Fuchs, B., Gruber-Vodicka, H.R., Hach, P.F., Littmann, S., Schoffelen, N.J.,
323 Kalvelage, T., Thomsen, S. and Schunck, H.: Oxygen minimum zone cryptic sulfur cycling sustained by offshore transport of
324 key sulfur oxidizing bacteria, *Nat. Commun.*, 9(1), 1-11, <https://doi.org/10.1038/s41467-018-04041-x>, 2018.
- 325 Canfield, D.E., Stewart, F.J., Thamdrup, B., De Brabandere, L., Dalsgaard, T., Delong, E.F., Revsbech, N.P. and Ulloa, O.: A
326 cryptic sulfur cycle in oxygen-minimum-zone waters off the Chilean coast, *Science*, 330(6009), 1375-1378, DOI:
327 10.1126/science.1196889, 2010.
- 328 Codispoti, L. A.: An oceanic fixed nitrogen sink exceeding 400 Tg N a⁻¹ vs the concept of homeostasis in the fixed-nitrogen
329 inventory, *Biogeosciences*, 4, 233–253, <https://doi.org/10.5194/bg-4-233-2007>, 2007.
- 330 Codispoti, L. A., Brandes, J. A., Christensen, J. P., Devol, A. H., Naqvi, S. W. A., Paerl, H. W., and Yoshinari, T.: The oceanic
331 fixed nitrogen and nitrous oxide budgets: Moving targets as we enter the anthropocene?, *Sci. Mar.*, 65(S2), 85-105, 2007.
- 332 Dall'Olmo, G., and Mork, K. A.: Carbon export by small particles in the Norwegian Sea, *Geophys. Res. Lett.*, 41, 2921–2927,
333 <https://doi.org/10.1002/2014GL059244>, 2014.
- 334 Dalsgaard, T., Stewart, F.J., Thamdrup, B., De Brabandere, L., Revsbech, N.P., Ulloa, O., Canfield, D.E. and DeLong, E.F.:
335 Oxygen at nanomolar levels reversibly suppresses process rates and gene expression in anammox and denitrification in the
336 oxygen minimum zone off northern Chile, *MBio.*, 5(6), e01966-14, 10.1128/mBio.01966-14, 2014.
- 337 Dalsgaard, T., Thamdrup, B., Farías, L., and Revsbech, N. P.: Anammox and denitrification in the oxygen minimum zone of
338 the eastern South Pacific, *Limnol. Oceanogr.*, 57(5), 1331-1346, <https://doi.org/10.4319/lo.2012.57.5.1331>, 2012.
- 339 de Boyer Montégut, C., Madec, G., Fischer, A. S., Lazar, A., and Iudicone, D.: Mixed layer depth over the global ocean: An
340 examination of profile data and a profile-based climatology, *J. Geophys. Res. Oceans*, 109(C12),
341 <https://doi.org/10.1029/2004JC002378>, 2004.
- 342 DeVries, T., Deutsch, C., Primeau, F., Chang, B., and Devol, A.: Global rates of water-column denitrification derived from
343 nitrogen gas measurements, *Nat. Geosci.*, 5(8), 547-550, <https://doi.org/10.1038/ngeo1515>, 2012.
- 344 Estapa, M. L., Feen, M. L., and Breves, E.: Direct observations of biological carbon export from profiling floats in the
345 subtropical North Atlantic, *Global Biogeochem. Cy.*, 33(3), 282-300, <https://doi.org/10.1029/2018GB006098>, 2019.
- 346 Fuchsman, C. A., Devol, A. H., Saunders, J. K., McKay, C., and Rocab, G.: Niche partitioning of the N cycling microbial
347 community of an offshore oxygen deficient zone, *Front. Microbiol.*, 8, 2384, <https://doi.org/10.3389/fmicb.2017.02384>, 2017.
- 348 Fuchsman, C. A., Murray, J. W., and Konovalov, S. K.: Concentration and natural stable isotope profiles of nitrogen species
349 in the Black Sea, *Mar. Chem.*, 111(1-2), 90-105, <https://doi.org/10.1016/j.marchem.2008.04.009>, 2008.
- 350 Fuchsman, C. A., Murray, J. W., and Staley, J. T.: Stimulation of autotrophic denitrification by intrusions of the Bosphorus
351 Plume into the anoxic Black Sea, *Front. Microbiol.*, 3, 257, <https://doi.org/10.3389/fmicb.2012.00257>, 2012b.



- 352 Fuchsman, C. A., Paul, B., Staley, J. T., Yakushev, E. V., and Murray, J. W.: Detection of transient denitrification during a
353 high organic matter event in the Black Sea, *Global Biogeochem. Cy.*, 33(2), 143-162, <https://doi.org/10.1029/2018GB006032>,
354 2019.
- 355 Fuchsman, C. A., Staley, J. T., Oakley, B. B., Kirkpatrick, J. B., and Murray, J. W.: Free-living and aggregate-associated
356 Planctomycetes in the Black Sea, *FEMS Microbiol. Ecol.*, 80(2), 402-416, <https://doi.org/10.1111/j.1574-6941.2012.01306.x>,
357 2012a.
- 358 Ganesh, S., Bristow, L. A., Larsen, M., Sarode, N., Thamdrup, B., and Stewart, F. J.: Size-fraction partitioning of community
359 gene transcription and nitrogen metabolism in a marine oxygen minimum zone, *ISME J.*, 9(12), 2682,
360 <https://doi.org/10.1038/ismej.2015.44>, 2015.
- 361 Ganesh, S., Parris, D. J., DeLong, E. F., and Stewart, F. J.: Metagenomic analysis of size-fractionated picoplankton in a marine
362 oxygen minimum zone, *ISME J.*, 8(1), 187, <https://doi.org/10.1038/ismej.2013.144>, 2014.
- 363 Gaye, B., Nagel, B., Dähnke, K., Rixen, T., and Emeis, K. C.: Evidence of parallel denitrification and nitrite oxidation in the
364 ODZ of the Arabian Sea from paired stable isotopes of nitrate and nitrite, *Global Biogeochem. Cy.*, 27(4), 1059-1071,
365 <https://doi.org/10.1002/2011GB004115>, 2013.
- 366 Gruber, N., and Sarmiento, J. L.: Global patterns of marine nitrogen fixation and denitrification, *Global Biogeochem. Cy.*,
367 11(2), 235-266, <https://doi.org/10.1029/97GB00077>, 1997.
- 368 Gruber, N., and Galloway, J. N.: An Earth-system perspective of the global nitrogen cycle, *Nature*, 451(7176), 293-296,
369 <https://doi.org/10.1038/nature06592>, 2008.
- 370 Hamme, R. C., and Emerson, S. R.: The solubility of neon, nitrogen and argon in distilled water and seawater, *Deep-Sea Res.*
371 *Pt. I.*, 51(11), 1517-1528, <https://doi.org/10.1016/j.dsr.2004.06.009>, 2004.
- 372 Helm, K. P., Bindoff, N. L., and Church, J. A.: Observed decreases in oxygen content of the global ocean, *Geophys. Res. Lett.*,
373 38(23), <https://doi.org/10.1029/2011GL049513>, 2011.
- 374 Jayakumar, A., Chang, B. X., Widner, B., Bernhardt, P., Mulholland, M. R., and Ward, B. B.: Biological nitrogen fixation in
375 the oxygen-minimum region of the eastern tropical North Pacific ocean, *ISME J.*, 11(10), 2356-2367,
376 <https://doi.org/10.1038/ismej.2017.97>, 2017.
- 377 Jensen, M. M., Kuypers, M. M., Gaute, L., and Thamdrup, B.: Rates and regulation of anaerobic ammonium oxidation and
378 denitrification in the Black Sea, *Limnol. Oceanogr.*, 53(1), 23-36, <https://doi.org/10.4319/lo.2008.53.1.0023>, 2008.
- 379 Johnson, K. S.: Manganese redox chemistry revisited. *Science*, 313(5795), 1896-1897, DOI: 10.1126/science.1133496, 2006.
- 380 Johnson, K. S., Pasqueron de Fommervault, O., Serra, R., D'Ortenzio, F., Schmechtig, C., Claustre, H., and Poteau, A.:
381 Processing Bio-Argo nitrate concentration at the DAC level, doi:10.13155/46121, 2018.
- 382 Karl, D. M., Church, M. J., Dore, J. E., Letelier, R. M., and Mahaffey, C.: Predictable and efficient carbon sequestration in the
383 North Pacific Ocean supported by symbiotic nitrogen fixation, *Proc. Natl. Acad. Sci. U. S. A.*, 109(6), 1842-1849,
384 <https://doi.org/10.1073/pnas.1120312109>, 2012.



- 385 Karl, D. M., Knauer, G. A., and Martin, J. H.: Downward flux of particulate organic matter in the ocean: a particle
386 decomposition paradox, *Nature*, 332(6163), 438-441, <https://doi.org/10.1038/332438a0>, 1988.
- 387 Karstensen, J., Stramma, L., and Visbeck, M.: Oxygen minimum zones in the eastern tropical Atlantic and Pacific oceans,
388 *Prog. Oceanogr.*, 77(4), 331-350, <https://doi.org/10.1016/j.pocean.2007.05.009>, 2008.
- 389 Keeling, R. F., and Garcia, H. E.: The change in oceanic O₂ inventory associated with recent global warming, *Proc. Natl. Acad.*
390 *Sci. U. S. A.*, 99(12), 7848-7853, <https://doi.org/10.1073/pnas.122154899>, 2002.
- 391 Kiko, R., Biastoch, A., Brandt, P., Cravatte, S., Hauss, H., Hummels, R., Kriest, I., Marin, F., McDonnell, A.M.P., Oschlies,
392 A. and Picheral, M.: Biological and physical influences on marine snowfall at the equator, *Nat. Geosci.*, 10(11), 852-858,
393 <https://doi.org/10.1038/ngeo3042>, 2017.
- 394 Kirkpatrick, J. B., Fuchsman, C. A., Yakushev, E., Staley, J. T., and Murray, J. W.: Concurrent activity of anammox and
395 denitrifying bacteria in the Black Sea, *Front. Microbiol.*, 3, 256, <https://doi.org/10.3389/fmicb.2012.00256>, 2012.
- 396 Konovalov, S.K., Luther, G.I.W., Friederich, G.E., Nuzzio, D.B., Tebo, B.M., Murray, J.W., Oguz, T., Glazer, B., Trouwborst,
397 R.E., Clement, B. and Murray, K.J.: Lateral injection of oxygen with the Bosphorus plume—fingers of oxidizing potential in
398 the Black Sea, *Limnol. Oceanogr.*, 48(6), 2369-2376, <https://doi.org/10.4319/lo.2003.48.6.2369>, 2003.
- 399 Konovalov, S. K., Murray, J. W., and Luther III, G. W.: Black Sea Biogeochemistry, *Oceanography*, 18(2), 24,
400 <https://doi.org/10.5670/oceanog.2005.39>, 2005.
- 401 Konovalov, S. K., Murray, J. W., Luther, G. W., and Tebo, B. M.: Processes controlling the redox budget for the oxic/anoxic
402 water column of the Black Sea, *Deep-Sea Res. Pt. II.*, 53(17-19), 1817-1841, <https://doi.org/10.1016/j.dsr2.2006.03.013>, 2006.
- 403 Kuypers, M.M., Sliemers, A.O., Lavik, G., Schmid, M., Jørgensen, B.B., Kuenen, J.G., Damsté, J.S.S., Strous, M. and Jetten,
404 M.S.: Anaerobic ammonium oxidation by anammox bacteria in the Black Sea, *Nature*, 422(6932), 608,
405 <https://doi.org/10.1038/nature01472>, 2003.
- 406 Lam, P., Lavik, G., Jensen, M.M., van de Vossenberg, J., Schmid, M., Woebken, D., Gutiérrez, D., Amann, R., Jetten, M.S.
407 and Kuypers, M.M.: Revising the nitrogen cycle in the Peruvian oxygen minimum zone, *Proc. Natl. Acad. Sci. U. S. A.*,
408 106(12), 4752-4757, <https://doi.org/10.1073/pnas.0812444106>, 2009.
- 409 Margolin, A. R., Gerringa, L. J., Hansell, D. A., and Rijkenberg, M. J.: Net removal of dissolved organic carbon in the anoxic
410 waters of the Black Sea, *Mar. Chem.*, 183, 13-24, <https://doi.org/10.1016/j.marchem.2016.05.003>, 2016.
- 411 Murray, J. W., Codispoti, L. A., and Friederich, G. E.: Oxidation-reduction environments: The suboxic zone in the Black Sea,
412 In C. P. Huang, C. R. O'Melia, and J. J. Morgan (Eds.), *Aquatic chemistry: Interfacial and interspecies processes*, ACS
413 *Advances in Chemistry Series* (Vol. 224, pp. 157-176), Washington DC: American Chemical Society, 1995.
- 414 Naqvi, S.W.A.: Geographical extent of denitrification in the Arabian Sea, *Oceanol. Acta*, 14(3), 281-290, 1991
- 415 Naqvi, S. W. A., Kumar, M. D., Narvekar, P. V., De Sousa, S. N., George, M. D., and D'silva, C.: An intermediate nepheloid
416 layer associated with high microbial metabolic rates and denitrification in the northwest Indian Ocean, *J. Geophys. Res.*
417 *Oceans*, 98(C9), 16469-16479, <https://doi.org/10.1029/93JC00973>, 1993.



- 418 Organelli, E., Dall'Olmo, G., Brewin, R. J., Tarran, G. A., Boss, E., and Bricaud, A.: The open-ocean missing backscattering
419 is in the structural complexity of particles, *Nat. Commun.*, 9(1), 1–11. <https://doi.org/10.1038/s41467-018-07814-6>, 2018.
- 420 Oschlies, A., Brandt, P., Stramma, L., and Schmidtko, S.: Drivers and mechanisms of ocean deoxygenation, *Nat. Geosci.*,
421 11(7), 467–473, <https://doi.org/10.1038/s41561-018-0152-2>, 2018.
- 422 Peters, B. D., Babbin, A. R., Lettmann, K. A., Mordy, C. W., Ulloa, O., Ward, B. B., and Casciotti, K. L.: Vertical modeling
423 of the nitrogen cycle in the eastern tropical South Pacific oxygen deficient zone using high-resolution concentration and isotope
424 measurements, *Global Biogeochem. Cy.*, 30(11), 1661–1681, <https://doi.org/10.1002/2016GB005415>, 2016.
- 425 Rasse, R., and Dall'Olmo, G.: Do oceanic hypoxic regions act as barriers for sinking particles? A case study in the eastern
426 tropical north Atlantic, *Global Biogeochem. Cy.*, <https://doi.org/10.1029/2019GB006305>, 2019.
- 427 Schmechtig, C., Claustre, H., Poteau, A., and D'Ortenzio, F.: Bio-Argo quality control manual for the chlorophyll-a
428 concentration, (pp.1–13), *Argo Data Management*. <https://doi.org/10.13155/35385>, 2014.
- 429 Schmechtig, C., Poteau, A., Claustre, H., D'Ortenzio, F., Giorgio Dall'Olmo, G., and Boss E.: Processing BGC-Argo particle
430 backscattering at the DAC level, <https://doi.org/10.13155/39459>, 2015.
- 431 Schmidtko, S., Stramma, L., and Visbeck, M.: Decline in global oceanic oxygen content during the past five decades. *Nature*,
432 542(7641), 335–339, <https://doi.org/10.1038/nature21399>, 2017.
- 433 Spinrad, R. W., Glover, H., Ward, B. B., Codispoti, L. A., and Kullenberg, G.: Suspended particle and bacterial maxima in
434 Peruvian coastal waters during a cold water anomaly, *Deep-Sea Res. Pt. I.*, 36(5), 715–733, 1989.
- 435 Stanev, E. V., Grayek, S., Claustre, H., Schmechtig, C., and Poteau, A.: Water intrusions and particle signatures in the Black
436 Sea: a Biogeochemical-Argo float investigation, *Ocean Dyn.*, 67(9), 1119–1136, <https://doi.org/10.1007/s10236-017-1077-9>,
437 2017.
- 438 Stanev, E. V., Poulain, P. M., Grayek, S., Johnson, K. S., Claustre, H., and Murray, J. W.: Understanding the Dynamics of the
439 Oxidic-Anoxic Interface in the Black Sea, *Geophys. Res. Lett.*, 45(2), 864–871, <https://doi.org/10.1002/2017GL076206>, 2018.
- 440 Stramma, L., Johnson, G. C., Sprintall, J., and Mohrholz, V.: Expanding oxygen-minimum zones in the tropical oceans.
441 *Science*, 320(5876), 655–658, <https://doi.org/10.1126/science.1153847>, 2008.
- 442 Stramski, D., Boss, E., Bogucki, D., and Voss, K. J.: The role of seawater constituents in light backscattering in the ocean.
443 *Prog. Oceanogr.*, 61(1), 27–56, <https://doi.org/10.1016/j.pocean.2004.07.001>, 2004.
- 444 Stramski, D., Reynolds, R. A., Kahru, M., and Mitchell, B. G.: Estimation of particulate organic carbon in the ocean from
445 satellite remote sensing, *Science*, 285(5425), 239–242, DOI: 10.1126/science.285.5425.239, 1999.
- 446 Thierry, V., Bittig, H., and Argo BGC Team.: Argo quality control manual for dissolved oxygen concentration. Version 2.0,
447 23 October 2018. [10.13155/46542](https://doi.org/10.13155/46542), 2018.
- 448 Tutasi, P., and Escribano, R.: Zooplankton diel vertical migration and downward C into the Oxygen Minimum Zone in the
449 highly productive upwelling region off Northern Chile, *Biogeosciences*, 17, 455–473, [https://doi.org/10.5194/bg-17-455-](https://doi.org/10.5194/bg-17-455-2020)
450 2020, 2020.



- 451 Ulloa, O., Canfield, D. E., DeLong, E. F., Letelier, R. M., and Stewart, F. J.: Microbial oceanography of anoxic oxygen
452 minimum zones, *Proc. Natl. Acad. Sci. U. S. A.*, 109(40), 15996-16003, <https://doi.org/10.1073/pnas.1205009109>, 2012.
- 453 Wang, W. L., Moore, J. K., Martiny, A. C., and Primeau, F. W.: Convergent estimates of marine nitrogen fixation, *Nature*,
454 566(7743), 205-211, <https://doi.org/10.1038/s41586-019-0911-2>, 2019.
- 455 Ward, B. B. How nitrogen is lost, *Science*, 341(6144), 352-353, DOI: 10.1126/science.1240314, 2013.
- 456 Ward, B.B., Devol, A.H., Rich, J.J., Chang, B.X., Bulow, S.E., Naik, H., Pratihary, A. and Jayakumar, A.: Denitrification as
457 the dominant nitrogen loss process in the Arabian Sea, *Nature*, 461(7260), 78-81, 2009.
- 458 Ward, B. B., Tuit, C. B., Jayakumar, A., Rich, J. J., Moffett, J., and Naqvi, S. W. A.: Organic carbon, and not copper, controls
459 denitrification in oxygen minimum zones of the ocean, *Deep-Sea Res. Pt. I.*, 55(12), 1672-1683,
460 <https://doi.org/10.1016/j.dsr.2008.07.005>, 2008.
- 461 Whitmire, A. L., Letelier, R. M., Villagrán, V., and Ulloa, O.: Autonomous observations of in vivo fluorescence and particle
462 backscattering in an oceanic oxygen minimum zone, *Opt. Express*, 17(24), 21, 992-22,004,
463 <https://doi.org/10.1364/OE.17.021992>, 2009.
- 464 Wojtasiewicz, B., Trull, T. W., Bhaskar, T. U., Gauns, M., Prakash, S., Ravichandran, M., and Hardman-Mountford, N. J.:
465 Autonomous profiling float observations reveal the dynamics of deep biomass distributions in the denitrifying oxygen
466 minimum zone of the Arabian Sea, *J. Mar. Syst.*, <https://doi.org/10.1016/j.jmarsys.2018.07.002>, 2018.